Primary joint statistical seismic influence on ionospheric parameters recorded by the CSES and DEMETER satellites

Mei Li, Xuhui Shen, Michel Parrot, Xuemin Zhang, Yan Zhang, Chen Yu, Rui Yan, Dapeng Liu, Hengxin Lu, Feng Guo, et al.

JGR Space Physics

RESEARCH ARTICLE
10.1029/2020JA028116

Key Points:
- This work presents primary statistical seismo-ionospheric influences by comparing different parameters and various time resolutions
- Different parameters and various time resolutions affect detection rate but independent of seismo-ionospheric influence evolution
- This study shows that the CSES could effectively register ionospheric perturbations due to strong EQs

Correspondence to:
M. Li,
mei_seis@163.com

Citation:
Li, M., Shen, X., Parrot, M., Zhang, X., Zhang, Y., Yu, C., et al. (2020). Primary joint statistical seismic influence on ionospheric parameters recorded by the CSES and DEMETER satellites. *Journal of Geophysical Research: Space Physics*, *125*, e2020JA028116. https://doi.org/10.1029/2020JA028116

Received 19 APR 2020
Accepted 23 JUL 2020
Accepted article online 16 NOV 2020

Primary Joint Statistical Seismic Influence on Ionospheric Parameters Recorded by the CSES and DEMETER Satellites

Mei Li[1], Xuhui Shen[2], Michel Parrot[3], Xuemin Zhang[4], Yan Zhang[1], Chen Yu[1], Rui Yan[2], Dapeng Liu[2], Hengxin Lu[2], Feng Guo[2], and Jianping Huang[2]

[1]China Earthquake Networks Center, China Earthquake Administration, Beijing, China, [2]National Institute of Natural Hazards, Ministry of Emergency Management of China, Beijing, China, [3]Laboratoire de Physique et Chimie de l'Environnement et de l'Espace, Université d'Orléans, CNRS, Orléans, France, [4]Institute of Earthquake Forecasting, China Earthquake Administration, Beijing, China

Abstract Oppositely to a previous statistical work using a single time resolution of the total ion density measured onboard the Detection of Electro-Magnetic Emissions Transmitted from Earthquake Regions (DEMETER) satellite, this work deals with statistical seismo-ionospheric influences by comparing different parameters and various time resolutions. The O^+ density and electron density recorded by the China Seismo-Electromagnetic Satellite (CSES) for more than one year and by the DEMETER satellite for about 6.5 years have been utilized to globally search ionospheric perturbations with different time resolutions. A comparison is automatically done by software between the occurrence of these ionospheric perturbations determined by different data sets, and the occurrence of earthquakes under the conditions that these perturbations occur at less than 1,500 km and up to 15 days before the earthquakes. Combined with statistical results given by both satellites, it is shown that the detection rate *r* of earthquakes increases as the data time resolution and the earthquake magnitude increase and as the focal depth decreases. On average, the number of perturbations is higher the day of the earthquake, and then smoothly decreases the days before, which is independent of either ionospheric parameters or time resolutions. The number of right alarms is high near the South Atlantic Magnetic Anomaly area but its relationship with seismic activities is weak. The ion density tends to be more sensitive to seismic activities than the electron density but this needs further investigations. This study shows that the CSES could effectively register ionospheric perturbations due to strong EQs as the DEMETER satellite does.

1. Introduction

With the development of Earth observation satellites, their onboard experiments have gradually shown their potential application in the field of earthquake (EQ) monitoring and investigation. This is due to their advantages of fast-speed, large-scale, and high-resolution results, especially for areas with harsh natural conditions. On one hand, scientific data from satellites have been utilized to distinguish precursors prior to strong EQs. As one result of researches during the last ten years, it has been shown that the ionosphere is unexpectedly sensitive to the seismic activity (Hayakawa & Molchanov, 2002). On the other hand, these satellite data have also been combined with ground-based observations to study the lithosphere-atmosphere-ionosphere coupling (Hayakawa & Molchanov, 2002; Li et al., 2016, 2019; Molchanov et al., 2004; Molchanov & Hayakawa, 2008; Pulinets et al., 1994, 1997, 2000; Pulinets & Ouzounov, 2011; Sorokin et al., 2015, and references therein).

Irregularities in the ionospheric sounder data before the Alaskan earthquake taking place on 28 March 1964 were reported as early as 1965 (Davies & Baker, 1965). However, examples have been recently intensively reported about seismic influence on different ionospheric parameters as modern satellite-borne receivers develop, especially after the launch of the DEMETER (Detection of Electro-Magnetic Emissions Transmitted from Earthquake Regions) satellite in 2004 in France. Ionospheric variations have been confirmed before the L'Aquila M_S 6.2 EQ on 6 April 2009 on GPS TEC (total electron content) and DEMETER IAP (Instrument d'Analyse du Plasma) ion density and ISL (Instrument Sonde de Langmuir) electron density (Akhoondzadeh et al., 2010; Stangl & Boudjada, 2011). Notably, multiparameter

ionospheric changes have also been reported prior to the huge Wenchuan M_S 8.0 EQ on 12 May 2008 including (i) the $f0F_2$ (critical frequency of the F_2 layer) values measured by ground-based sounders, and the very low frequency (VLF) fields (Ding et al., 2010; Maurya et al., 2013; Sun et al., 2011; Xu, Hu, Wu, Suo, et al., 2010; Xu, Hu, Wu, Wu, et al., 2010; Xu et al., 2011; Yu et al., 2009; Zhao et al., 2008); (ii) the ion density, electron density, electron temperature, ULF (ultralow frequency), VLF, and ELF (extremely low frequency) electric fields, O^+ density, ion temperature, and energetic particle measured by DEMETER (Akhoondzadeh et al., 2010; An et al., 2010; BŁEÇKI et al., 2010; He et al., 2011a, 2011b; Liu et al., 2015; Onishi et al., 2011; Ryu et al., 2014; Sarkar & Gwal, 2010; Walker et al., 2013; Wan et al., 2012; Yan et al., 2012; Zeng et al., 2009; Zhang, Shen, Liu, et al., 2009; Zhang, Shen, Ouyang, et al., 2009); (iii) the TEC measured by GPS satellites (Akhoondzadeh et al., 2010; Lin et al., 2009; Liu, Chou, et al., 2009; Ma et al., 2014; Pulinets & Ouzounov, 2011; Pulinets et al., 2009; Ryu et al., 2014; Yan et al., 2012; Yu et al., 2009; Zhao et al., 2008, 2010; Zhu et al., 2009); (iv) the TEC and NmF_2 (electron density at F_2 peak) values measured by radio occultation using the six microsatellites FORMOSAT3/COSMIC (F3/C) (Hsiao et al., 2010; Liu, Chen, et al., 2009; Ma et al., 2014); and (v) the electron density measured by the CHAMP (challenging minisatellite payload) satellite (Ryu et al., 2014). This shows that various ionospheric parameters measured by several scientific payloads onboard a satellite can response to a seismic event, especially for strong EQs.

There has been many statistical works on ionospheric variations associated with strong seismic events using satellite measurements. Seismo-ionospheric disturbances within a few days before EQs have been registered in 73% of EQs with magnitude 5.0, and in 100% of EQs with magnitude 6.0 (Pulinets et al., 2003). Liu, Chen, et al. (2009) have performed a statistical analysis on GPS TEC and found that seismo-ionospheric variations above the epicentral area occurred 5 days prior to 16 EQs out of 20 events with $M \geq 6.0$ in the Taiwan area from September 1999 to December 2002. Statistical analyses have also been performed using DEMETER data sets. A statistically significant decrease of wave intensity at 1.7 kHz during nighttime four hours before the occurrence of EQs has been reported respectively by Němec et al. (2008, 2009) and by Píša et al. (2012, 2013). Statistical analyses have been performed using a total ion density (the sum of H^+, He^+, and O^+) data set during the DEMETER lifetime (6.5 years) in the epicenter areas of earthquakes as well as in their magnetically conjugate point areas and the results have shown a significant statistical correlation between ionospheric anomalies and large events within a few days before the events (Li & Parrot, 2012, 2013, 2018; Parrot, 2011, 2012; Parrot & Li, 2017; Yan et al., 2017). Zhang et al. (2013) have found that there are increases in the number of electron bursts prior to strong EQs with a magnitude over 7.0 during the entire operation period of the DEMETER satellite. However, Akhoondzadeh et al. (2010) statistically analyzed the ionospheric variations prior to four large EQs simultaneously using, on one hand, several satellite parameters of DEMETER: IAP ion density and ion temperature, ISL electron density and electron temperature, and on the other hand, GPS TEC. Their results show that there is a very good agreement between the different parameters and that, most positive and negative anomalies appeared 1 to 5 days before all studied EQs during quiet geomagnetic conditions, although their amplitude depends on the magnitude of the EQs involved.

The CSES (China Seismo-Electromagnetic Satellite) has been launched for more than one year and effective payload data have been recorded. It is possible to check its response to seismic activities during this period. So, in this paper, a primary statistical analysis on seismo-ionospheric influence of different parameters of ion density and electron density recorded by CSES and DEMETER satellites will be comparatively shown. The CSES and DEMETER satellites are briefly described in section 2. In section 3, the data processing method is retrospectively introduced. In section 4, automatic statistical results for different parameters recorded by CSES will be compared with that of DEMETER and confirmed. Discussion and conclusions are provided in section 5.

2. The CSES and the DEMETER Satellite

The CSES was launched successfully on 2 February 2018. The CSES is a Sun-synchronous satellite orbiting at a height of 500 km with a circular orbit and the descending node happens at 14:00 local time (LT). There are eight scientific payloads onboard, including a search-coil magnetometer, an electric field detector, a high precision magnetometer, a plasma analyzer package, a Langmuir probe, an energetic particle detector, a GNSS occupation receiver, and a three-frequency beacon. Of these, the Langmuir probe (LAP) and plasma analyzer package (PAP) are the space plasma in situ detection payloads. Their scientific design parameters

can be referred to (Liu et al., 2018; Shen et al., 2018; Yan et al., 2018). The LAP allows access to the electron density and temperature. The operational modes of the LAP include survey mode and burst mode. The survey mode is used mainly to detect global electron density and electron temperature with sweeping period of 3 s (second), while the burst mode primarily allows detection of key areas, over China and within global main seismic belts with sweeping period of 1.5 s. The PAP measures ion density, composition, temperature, and flow velocity. PAP has also the same operational modes as that of LAP but with a little higher resolution of 1 s for survey mode and 0.5 s for burst.

DEMETER was launched in June 2004 onto a polar and circular orbit which measures electromagnetic waves and plasma parameters all around the globe except in the auroral zones (Parrot et al., 2006). DEMETER is a low-altitude satellite with an altitude of 710 km, which was decreased to 660 km in December 2005. The orbit of DEMETER is nearly sun-synchronous and the upgoing half-orbits correspond to night time (22.30 LT) whereas the downgoing half-orbits correspond to day time (10.30 LT). The onboard experiments of DEMETER includes six scientific payloads, the IAP—plasma analyzer instrument, the ICE—electric field instrument, the ISL—Langmuir probe, the IMSC—search-coil magnetometer instrument, the IDP—particle detector instrument, and the BANT—an electronic unit. The variations of the ion density and the electron density are measured by the instrument IAP and ISL, respectively. These two experiments have different operational modes. The ISL is with an experimental resolution of 1 s for all data, while the IAP has two experimental data resolutions of 4 s in survey mode and 2 s in burst mode. Details of the IAP and ISL experiments can be found in Berthelier et al. (2006) and Lebreton et al. (2006). The satellite's science mission has come to an end in December 2010.

3. Description of the Data Processing

3.1. Data

The O^+ is the main ion among the ions H^+, He^+, and O^+ detected by the satellites although it depends on some factors, such as, local time, altitude, and so on. So, the used data of CSES include PAP O^+ density and LAP electron density from 1 August 2018 to 30 November 2019. During this period, 4,317 strong EQs with magnitudes M_W equal to or more than 4.8 occurred (USGS: http://www.usgs.gov).

The DEMETER data used here include the completed data for the parameter IAP O^+ density and ISL electron density covering its lifetime from the mid-2004 to the end 2010. During this period (6.5 years in total) there are 21,863 strong EQs with magnitude $M_W \geq 4.8$ which took place (USGS: http://www.usgs.gov).

The Kp index (http://isgi.unistra.fr) is also checked in order to avoid the effect from the solar activities during all the periods considered in this paper.

3.2. Data Processing Method

The data processing method here is similar to the one used before by Li and Parrot (2012, 2013). First of all, a software is used to automatically search global ionospheric perturbations in several data sets (issued from CSES or DEMETER). Only the perturbations which comply with the duration time between 20 and 120 s are kept in the perturbation database but without a limit on perturbation amplitudes. Here, the minimum duration time 20 s is calculated automatically by the improved software according to data sample rate instead of previously used ~23 s, five data points for survey mode in IAP DEMETER (Li & Parrot, 2012, 2013). The information for each perturbation in the perturbation database includes peak appearing time, orbit number, location (latitude and longitude), background value, amplitude, change trend (increase or decrease; if the amplitude is larger than the background value, it is increase, if not, it is decrease), increase or decrease percentage, duration time, and extension distance (km).

In order to examine the capability of recording seismic influence on the ionosphere with different data time resolutions using our software, the raw data are sampled at different time resolutions: 1 and 3 s for PAP O^+ density and 3 s for LAP electron density of CSES; 4 s for IAP O^+ density, and 3 and 4 s for ISL electron density of DEMETER. Thus, six data sets have been established: PAP-1 s, PAP-3 s, and LAP-3 s for CSES; IAP-4 s, ISL-3 s, and ISL-4 s for DEMETER. At the same time, the SAVGOL method is employed to smooth the data before searching for perturbations. The SAVGOL function returns the coefficients of a Savitzky-Golay smoothing filter (Savitzky & Golay, 1964). So, at this stage, two O^+ perturbation databases (1 and 3 s data are used respectively, including 48,529 and 24,438 perturbations in total) and one electron database

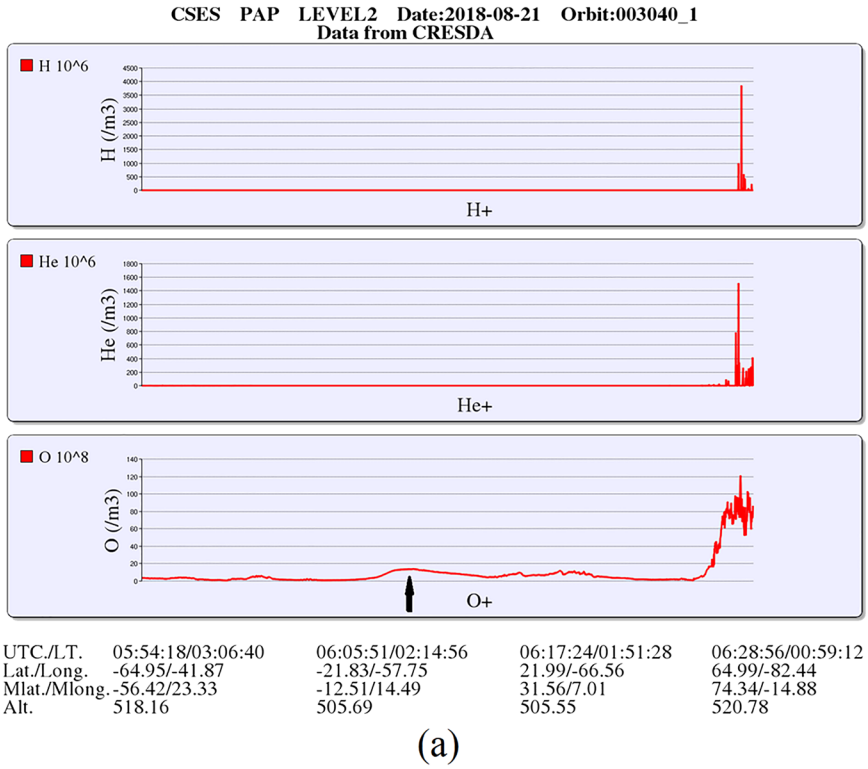

(a)

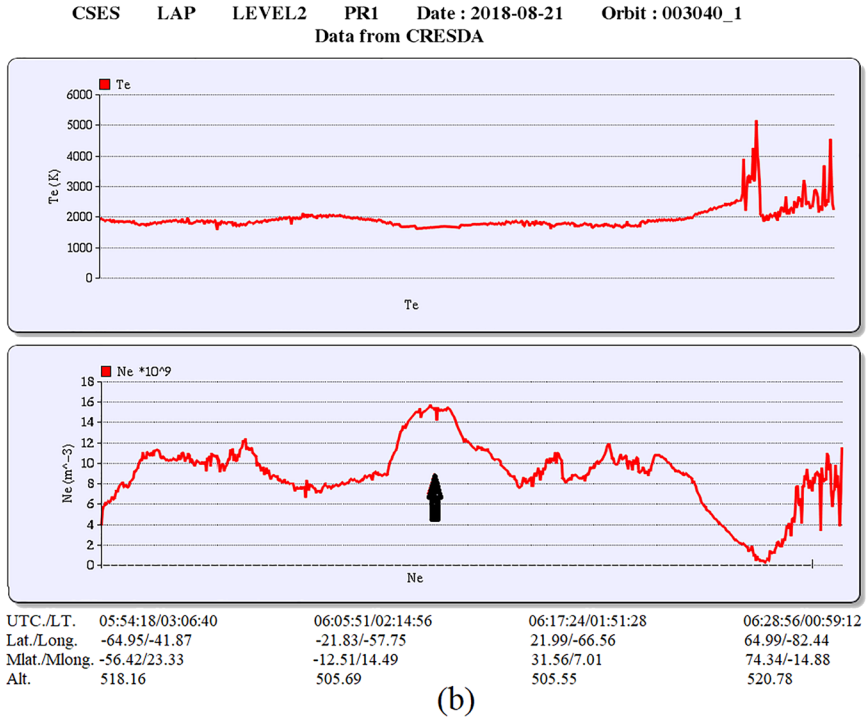

(b)

Figure 1. Data recorded on 21 August 2018 between 05.54.18 and 06.28.56 UT, 15 h before a M_W 7.3 EQ along the orbit 03040_1. (a) Variations of ion densities recorded by PAP onboard the CSES. The panels from the top to the bottom are H^+ density, He^+ density, and O^+ density. An increase has been labeled by a black arrow in O^+ curve and it looks not obvious because of large scale of *Y* axis coordinate. In fact, the automatic detection indicates that this increase amplitude is about 29%. (b) Variations of electron data recorded by LAP onboard the CSES. The top panel is the electron temperature (Te) and the bottom one is the electron density (Ne) with an apparent 21.9% increase labeled by a black arrow. The parameters below the plots indicate the time in UT/LT and the position of the satellite along its orbit.

Table 1
Information on the PAP Ion Density and the LAP Electron Density Perturbations Shown in Figure 1 and Automatically Detected by the Software

PAP O^+ density perturbation	LAP electron density perturbation
Time: 2018 8 21 6 15 31 712	Time: 2018 8 21 6 15 26 856
Orbit: 3040	Orbit: 3040
Suborbit: 1	Suborbit: 1
Latitude: 14.5951	Latitude: 14.5468
Longitude: −65.0325	Longitude: −65.0051
BkgdIon ($10^6/m^3$): 336.602	BkgdElectron ($10^6/m^3$): 8473.04
Amplitude ($10^6/m^3$): 434.302	Amplitude ($10^6/m^3$): 10332.1
Trend: Increase	Trend: Increase
Percent: 29.0254	Percent: 21.9409
Time_width (m s ms): 1 27 1	Time_width (m s ms): 1 57 0
Extension (km): 619.000	Extension (km): 837.000

(3 s data, 26,782 perturbations) for CSES, and one O^+ perturbation database (4 s data, 74,959 perturbations) and two electron databases (3 and 4 s data, 44,285 and 32,627 perturbations) for DEMETER have been established.

After, a second software is used to check whether the ionospheric perturbations are corresponding to an EQ or not under the following three limits, (i) the Kp index is kept to be less than 3 in order to reduce the effect of the geomagnetic activity on the ionosphere. This geomagnetic activity is induced by solar magnetic storms, (ii) the distance (D) between the location of the perturbation on the orbit and the epicenter is equal to or less than 1,500 km, and (iii) the delay time (T) before an EQ is equal to or less than 15 days. If an earthquake is corresponding to one or to more than one perturbation, we consider it is a good detection; if not, it is a bad detection. If a perturbation corresponds to an earthquake, it is a right alarm; if not, it is a false alarm. More details can also be found in Parrot and Li (2017) and Li and Parrot (2018).

An example of ionospheric perturbation detected by the software and corresponding to an EQ is shown in Figure 1. It corresponds to an EQ occurring on 21 August 2018 at 21:31:47 UT with a magnitude equal to M_W 7.3 and a depth equal to 147 km. Its position was 10.77°N, 62.90°W. Figure 1a shows variations of PAP parameters. From the top to the bottom, the panels show the densities of the H^+, He^+, and O^+ ion. The X axis represents UTC (Universal Time Coordinated)/BJT (Beijing time), latitude, longitude, and altitude of CSES. At 6:00 UT, about 15 h before this EQ, the orbit 03040 flew up this epicentral area and an increase of O^+ labeled by a black arrow in the bottom panel with red curve is observed in Figure 1a (this variation seems not obvious at this period because it is formed automatically by the CSES data processing system). Correspondingly, the payload LAP also recorded clear increase of electron density on the same orbit as it is shown in the bottom panel with a black arrow in Figure 1b.

These two ionospheric perturbations of PAP and LAP have been successfully detected by the software and their information is shown in Table 1. From Table 1, one can see that these two ionospheric perturbations

Table 2
Detected Rates r for Different Groups of EQs and Different Data Sets (PAP-1 s, PAP-3 s, and LAP-3 s) Recorded by CSES (D = 1,500 km, T = 15 days)

		$4.8 \le M \le 5.0$	$5.0 < M \le 6.0$	$M > 6.0$	Zone1	Zone2
Data set	d	r	r	r	r	r
PAP-1 s	0–1,000	54.5%	61.1%	89.9%	63.2%	46.4%
	0–20	64.1%	67.5%	87.0%	66.4%	50.1%
PAP-3 s	0–1,000	45.4%	53.1%	87.6%	56.8%	35.0%
	0–20	56.3%	61.3%	87.0%	59.4%	50.0%
LAP-3 s	0–1,000	45.4%	51.5%	85.2%	61.1%	42.0%
	0–20	56.4%	59.7%	84.4%	67.2%	46.6%

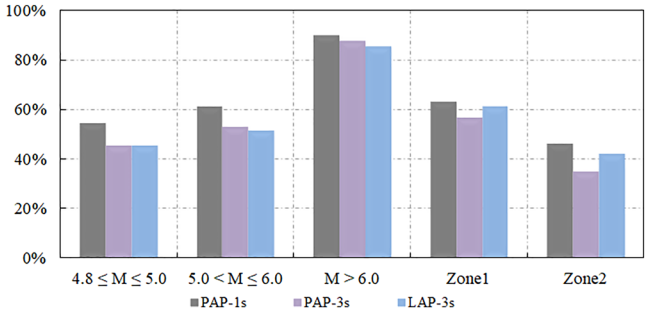

Figure 2. Histogram of EQ detection rates for different groups of EQs: $4.8 \leq M \leq 5.0$, $5.0 < M \leq 6.0$, $M > 6.0$, Zone1, and Zone2. Each group of EQs are detected under the conditions of $D = 1{,}500$ km, $T = 15$ days, and the focal depth $d = 0$–$1{,}000$ km with different ionospheric databases confirmed by data sets of PAP-1 s and PAP-3 s data and LAP-3 s from CSES. The time period is from August 2018 to November 2019 as CSES flies.

almost occurred at the same time, and then the two peaks have a very near location (477 and 483 km away from the epicenter of this M_W7.3 EQ). The corresponding increases relatively to the background values are larger than 20%.

4. Statistical Seismo-ionospheric Influences

4.1. EQ Detection Rate

Here, a parameter r is defined as the EQ detection rate, which is the ratio of the number of EQs detected corresponding to one or more than one ionospheric perturbations and the number of EQs which comply with the limit conditions.

EQs are still divided into different groups during this work in order to gain an easy comparison as properties of EQs vary. The 4,317 $M_W \geq 4.8$ EQs occurring between August 2018 and November 2019 as CSES flies have been divided into three groups according to their magnitudes: $4.8 \leq M_W \leq 5.0$ 2524 EQs, $5.0 < M_W \leq 6.0$ 1624 EQs, and $M_W > 6.0$ 169 EQs. Then, in light of previous statistical seismo-ionospheric influences for EQs located in different areas of the world (see, e.g., the effect of the South Atlantic Magnetic Anomaly (SAMA) on EQ detection reported by Li and Parrot (2012, 2013)), two specific rectangular zones have been selected (see Figure 6 in section 5), (i) a Zone1 with latmin = −70°, latmax = −45°, longmax = 150°W, longmin = 20°W, which lies in the SAMA area in south hemisphere and includes 190 EQs, and (ii) a Zone2 with latmin = 0°, latmax = 30°, longmin = 90°E, longmax = 150°E, which lies in low-middle latitude in north hemisphere and includes 774 EQs. For each group of EQs, they are detected under the conditions of $D = 1{,}500$ km, $T = 15$ days, and the focal depth $d = 0$–$1{,}000$ km with different ionospheric databases confirmed by data sets of PAP-1 s and PAP-3 s data and LAP-3 s from CSES. To check effects of the focal depth (d) of earthquakes on the detection rate, "crust" earthquakes with $d \leq 20$ km have been comparatively detected for each group of EQs. The Kp index is kept to be less than 3 during this period in order to eliminate the effect from solar activities. Their corresponding detection rates are listed in Table 2.

From Table 2, except $M > 6.0$ with contrary result due to its less examples (169 in total and 77 with the depth $d \leq 20$ km), the detection rate r for "crust" EQs with $d = 0$–20 km is thoroughly higher than that of EQs with $d = 0$–$1{,}000$ km for each group of EQs in all data sets. These results tend to verify a definite conclusion that ionospheric influence can be affected by the epicenter depth: The "crust" EQs can be easily detected than "deep" ones, which has been already reported by Li and Parrot (2012) and Silina et al. (2001).

For a better comparison, the data in Table 2 with $d = 0$–$1{,}000$ km have been shown in Figure 2 under the form of histograms.

From Table 2 and Figure 2, it is clear that the detection rate r increases as the magnitude of EQs increases. Additionally, for the same parameter PAP O^+ density with different data time resolutions of 1 and 3 s, the detection rates of PAP-1 s for six group EQs of $4.8 \leq M_W \leq 5.0$, $5.0 < M_W \leq 6.0$, $M_W > 6.0$, Zone1, and Zone2 are higher than that of PAP-3 s, which means that the detection rate r increases as the time resolution of data increases; for different parameters of PAP O^+ density and LAP electron density with the same time

Table 3
Detected Rates for Different Groups of EQs and Different Time Resolutions of Perturbations Recorded by DEMETER ($D = 1{,}500$ km, $T = 15$ days, $d = 0$–$1{,}000$ km)

Data set	$4.8 \leq M \leq 5.0$	$5.0 < M \leq 6.0$	$M > 6.0$	Zone1	Zone2
	r	r	r	r	r
ISL-3 s	37.3%	43.0%	68.3%	65.7%	11.8%
ISL-4 s	31.0%	36.7%	57.9%	58.7%	9.4%
IAP-4 s	49.5%	55.1%	76.7%	63.4%	17.0%

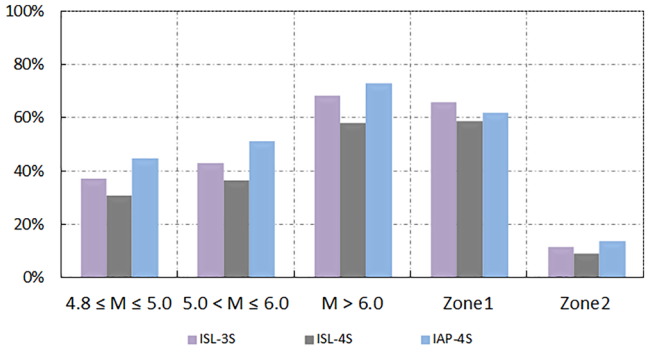

Figure 3. Histogram of detection rates using different time resolution data of IAP 4 s and ISL 3 and 4 s recorded by DEMETER for different groups of EQs: $4.8 \leq M_W \leq 5.0$, $5.0 < M_W \leq 6.0$, $M_W > 6.0$, Zone1, and Zone2. The time period corresponds to the lifetime of DEMETER.

resolution of 3 s, detection rates of PAP for $4.8 \leq M_W \leq 5.0$, $5.0 < M_W \leq 6.0$, and $M_W > 6.0$ groups of EQs tend to be all higher a little than that of LAP but this law are contrary for the two group EQs of Zone1 and Zone2.

In order to confirm the results given by CSES, the 21863 EQs occurring during the DEMETER 6.5 year life time have been classified into six groups of EQs: $4.8 \leq M_W \leq 5.0$ 12057 EQs, $5.0 < M_W \leq 6.0$ 8953 EQs, $M_W > 6.0$ 853 EQs, Zone1 [70°S, 45°S] [150°W, 20°W] 615 EQs, and Zone2 [0°N, 30°N] [90°W, 150°W] 4,549 EQs. They are also detected with the same software under the conditions of $D = 1{,}500$ km, $T = 15$ days, and $d = 0$–$1{,}000$ km, and Kp < 3 with the different ionospheric perturbation databases named IAP-4 s, ISL-3 s, and ISL-4 s (see section 3.2). Their corresponding detection rates r are listed in Table 3.

For a better comparison, the data of Table 3 is shown in Figure 3 under the form of histograms.

From Table 3 and Figure 3, one thing we can reconfirm is that the detection rate r increases as the time resolution of the same ionospheric parameter ISL electron density increases.

Another point is that the detection rates for IAP density are clearly higher than that of ISL density for each group of EQs when the time resolution is the same, which probably gives a conclusion that the ion density is more sensitive to seismic activities than the electron density although this claim is not completely verified by the CSES data.

4.2. Temporal Evolution of Seismo-ionospheric Influences

To check the occurrence frequency of ionospheric perturbations during EQ preparation, a study has been conducted on the different cases, and the corresponding results are shown in Figure 4. Figure 4 displays the number of detected perturbations corresponding to an EQ (right alarms) as a function of days before the good detections considering the following data sets recorded by CSES: All EQs (4,317 EQs), $4.8 \leq M_W \leq 5.0$ EQs, Zone1, and Zone2. In each panel of Figure 4 the results are expressed as a percentage relative to the total number of right alarms within 15 days detected by PAP-1 s (red line), PAP-3 s (blue line), and LAP-3 s (orange line) data sets. In a similar way, Figure 5 is related to DEMETER and displays the relative

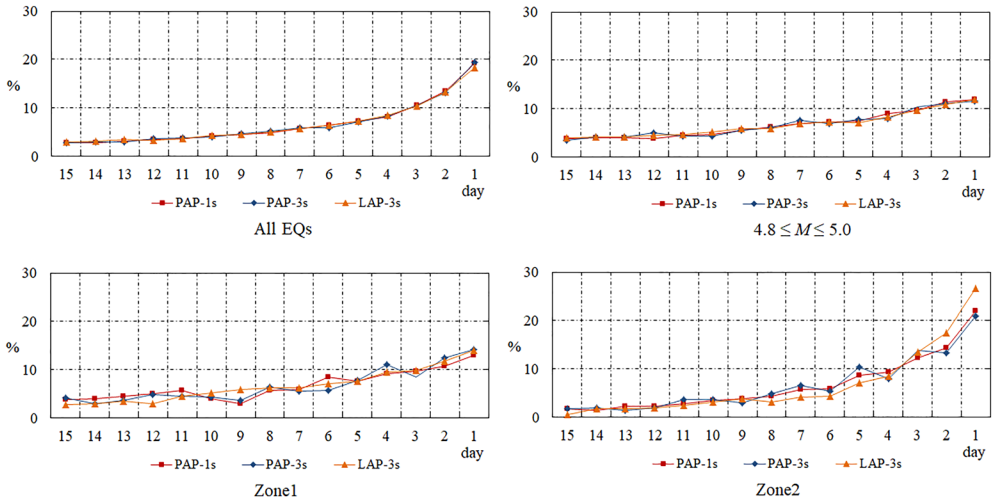

Figure 4. Variation of the number of perturbations as a function of the days before the EQs and for different cases (top left: all detected EQs, top right: detected EQs of $4.8 \leq M_W \leq 5.0$, bottom left: detected EQs in Zone1, and bottom right: detected EQs in Zone2). Each panel covers three groups of seismo-ionospheric influences determined by PAP-1 s (red line), PAP-3 s (blue line), and LAP-3 s (orange line) data sets recorded by CSES.

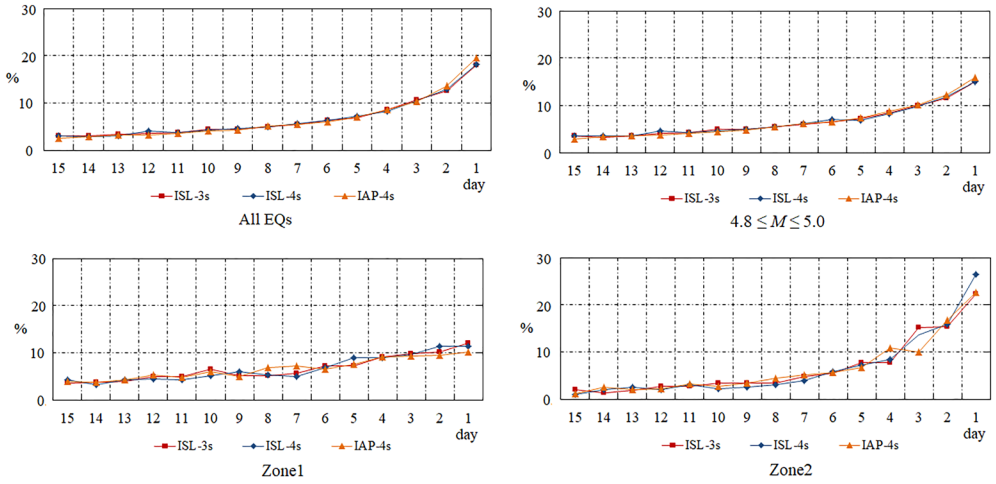

Figure 5. Variation of the number of perturbations as a function of the days before the EQs and for different cases (top left: all detected EQs, top right: detected EQs of $4.8 \leq M_W \leq 5.0$, bottom left: detected EQs in Zone1, and bottom right: detected EQs in Zone2). Each panel covers three groups of seismo-ionospheric influences determined by ISL-3 s (red line), ISL-4 s (blue line), and IAP-4 s (orange line) data sets recorded by DEMETER.

percentage each day before, considering: All EQs (21,863 EQs), $4.8 \leq M_W \leq 5.0$ EQs, Zone1, and Zone2. Each panel shows three percentage lines determined by the ISL-3 s (red line), ISL-4 s (blue line), and IAP-4 s (orange line) data sets.

It can be seen that, for all cases in Figures 4 and 5, the number of perturbations is maximum for days close to the EQ day and smoothly decreases when the time before the EQ is increasing. This is a variation that is intuitively expected. On one hand, this variation seems not mainly affected by the data time resolution of a given parameter whatever this parameter is. On the other hand, this trend becomes more obvious when the number of samples is large enough. Thus, three lines decay smoothly as day goes for All EQs (see the top left panel in Figures 4 and 5) but with a few fluctuations for other cases (see other panels also in Figures 4 and 5). However, the percentages increase more obviously in Zone2 (see the bottom right panel in Figures 4 and 5) than in Zone1 especially one week before the EQs. This means that the perturbations have a little relationship with seismic activity in the Zone1 area. In this case, false alarms become more important due to outer disturbances of the active $E \times B$ drift occurring in the South Atlantic Magnetic Anomaly (Abdu & Batista, 1977; Abdu et al., 2003, 2005).

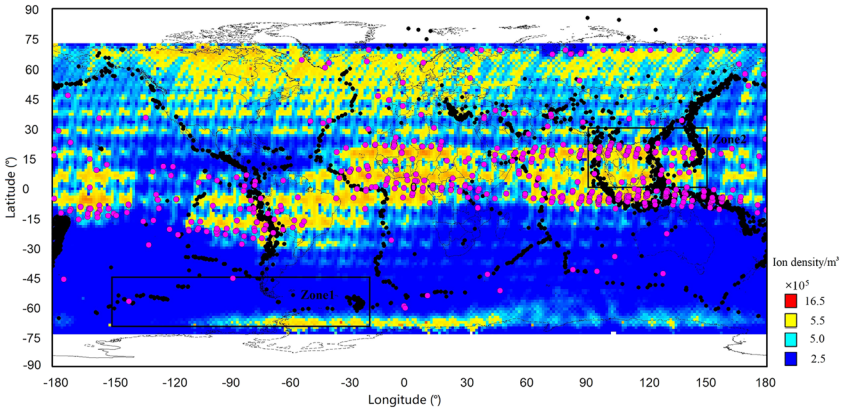

Figure 6. Distribution of large-scale ionospheric perturbations with a duration of 200–300 s (purple dots) automatically searched by software using PAP-1s data set from 1 August 2018 to 30 November 2019. Here, O^+ ion density recorded by CSES during October to December 2018 stands for a global ionospheric plasma variation. The main seismic zones in the world are basically determined by 4,317 EQs occurred during this period (black dots). Zone1 and Zone2 used above in section 4 have been labeled by two black empty rectangles.

5. Discussion and Conclusions

As CSES has run more than 1 year since it was launched on 2 February 2018 in China, this increases the probability to examine the effectiveness of seismo-ionospheric influences recorded by the scientific payloads of PAP O^+ density and LAP electron density. For comparison, two corresponding DEMETER parameters of IAP and ISL for about 6.5 years have also been checked to gain some similar results.

Oppositely to previous statistical works with DEMETER using a single time resolution of one parameter of IAP total ion density (Li & Parrot, 2012, 2013), this work is associated with statistical seismo-ionospheric influences using two parameters recorded by the DEMETER satellite and CSES, respectively. At the same time, various time resolutions for a given parameter are also employed to survey the effects of seismic activities on the ionosphere and also to check the efficiency of our two software.

Numerous investigations have shown that ionospheric variations generally appeared several days to two weeks prior to EQs. In this work, ionospheric perturbations are automatically searched with a delay time before an earthquake equal to or less than 15 days. The statistical results have displayed that totally the occurrence rate of these perturbations is the highest at the day of the earthquake and then gradually decreases at the day before. While this situation shows a different art of styles for groups of EQs due to regional influences, such as SAMA in Zone1. Relatively, Zone2 displays a more reliable result with averaged occurrence rates within one week (7 days) being 79.6% for all data sets. This result is highly coincident with some investigations that ionospheric variations mainly occurred several days prior to EQs (Akhoondzadeh et al., 2010; Liu, Chen, et al., 2009) and with the statistical work conducted by Li et al. (2019), who found that ionospheric variations mainly happened 6 days and gained a high climax 3 days before the Wenchuan main event on 12 May 2008 in the light of different authors (can be referred to Figure 4 in Li et al., 2019).

However, the abnormal range in the ionosphere arise from seismic activities has not been well established so far. The software in this paper is designed to only accept ionospheric perturbations with a duration of 20–120 s (about 160–840 km if the speed of the satellite 7.0 km/s is considered) and positive results have been given. In order to further examine this design is effective for the investigations, variations with a duration of 200–300 s using PAP-1s data set from August 1 2018 to November 30 2019 have been accepted this time and 509 ionospheric perturbations have been attained in total. These perturbations are located in the map of the world (see Figure 6 with purple dots). As a comparison, a global ionospheric plasma variation has been given by O^+ ion density recorded by CSES during this period and the main seismic zones in the world are basically determined by 4,317 EQs occurred during this period, which cover especially plate-boundary interfaces, Circum-Pacific seismic belt, and Chile seismic zone (black dots in Figure 6). Zone1 and Zone2 employed above in section 4 are also added to Figure 6 by two black empty rectangles.

From Figure 6, it is clear that these perturbations collect mainly around the equator. This distribution is not coincident with the main seismic belts of the world, but keeps the similar shape as the background distribution of ion density. These large-scale ionospheric dynamical variations near the equator have been formed arise from some complex origins, such as Equatorial plasma bubbles, which are extremely dynamical phenomena with density drop out more than an order of magnitude over distances of a few kilometers perpendicular to the magnetic field leading to large-scale ionospheric variations (Berthelier et al., 2006). At higher latitudes, more intense waves are characterized by auroral emissions duo to strong sources of ELF/VLF emissions (Lefeuvre et al., 1992).

In the equatorial and low midlatitude ionospheric regions, the distribution of plasma is controlled by the coupled processes of plasma diffusion, $E \times B$ drifts, thermospheric neutral winds and chemical processes (Horvath & Lovell, 2009). The daytime (nighttime) F region plasma is transported by a vertical upward (downward) $E \times B$ drift, created by interaction between the ionospheric E field and the geomagnetic B field, over the dip equator, and by field-aligned diffusions on both sides of the dip equator (Balan & Bailey, 1995; Balan et al., 1997; Hairston et al., 1997). These processes have a tendency to create a plasma distribution symmetric to the dip equator. However, this tendency is interrupted by the meridional and transequatorial neutral winds, which move the plasma along the magnetic field lines and produce hemispheric and interhemispheric plasma flows, respectively, and by the accompanying chemical processes (Bailey et al., 1997; Kil et al., 2006; Titheridge, 1995).

The results show that the detection rate r could be affected by the data time resolutions because high time resolution data can record small scale ionospheric variations. Thus, the detection rate tends to increase as the time resolution increases. For the same time resolution, the detection rate r determined by IAP O^+ density for all cases are always higher than that of ISL electron density on DEMETER (see Table 3 and Figure 3), but these results gained partly on CSES (see Table 2 and Figure 2) probably owing to a less number of samples. However, there are still a high false alarm number and a high bad detection number due to the fact that a single satellite cannot continuously survey a given area, and then the natural disturbances of the ionosphere. Thus, it seems that EQs in SAMA zone have a higher detection rate but the right alarms have a weak relationship to seismic activities (see bottom left panels in Figures 4 and 5).

However, over the South Atlantic, the total B field intensity is anomalously low ~22.8×10^3 nT from Trivedi et al. (2005), a phenomenon known as the South Atlantic Magnetic Anomaly (SAMA), that makes the $E \times B$ drift unusually strong, since its magnitude is $E \times B/B^2$ (Kendall & Pickering, 1967). Furthermore, there are special electrodynamic effects in the SAMA region that can further increase the magnitude of the $E \times B$ drift by increasing the E field. Because of these plasma dynamics, the plasma density is highly variable over the SAMA and can be anomalously low (Abdu et al., 2005). Due to energetic particle precipitations, there is an enhanced E layer ionization over the SAMA (Abdu & Batista, 1977). The E layer conductivity is a maximum, where the magnetic field is a minimum, at the center of the SAMA (310°E, 10°S in geographic coordinates), over south Brazil, and decreases with increasing distance away from that center, toward the African continent. This can result in a westward conductivity gradient over the SAMA (indicated as DS by Abdu et al., 2003) that can add to the background conductivity gradient, which is also westward directed during the postsunset hours. Thus, this can create a locally high (or modified) conductivity distribution that is a regular feature of the ionosphere over the SAMA (Abdu et al., 2005). According to their model simulations, this increased conductivity will create a significantly stronger vertical $E \times B$ at the prereversal enhancement over Brazil (east coast of South America) than over Jicamarca (west coast of South America). This combined to the fact that Zone1 is the seismic zone which is at the highest geomagnetic latitude make the number of ionospheric perturbations higher than in another seismic region.

Overall, the results given by CSES and DEMETER have shown the following:

1. The CSES ionospheric data can effectively respond to strong EQs.
2. The detection rate r increases as the time resolution of the satellite data, and the magnitude of EQs involved increase and decreases as the epicentral depth of seismic events increases.
3. On average, the occurring frequency of perturbations is higher the day of the EQ and then gradually decreases before the event. This is independent of the data sets we use, either the ion density or the electron density, and whatever are their time resolutions.
4. The ion density seems to be more sensitive to the seismic activities than the electron density, but it needs further investigations with more data.

However, there still leaves a large of number of false alarms although an earthquake is searched around 1,500 km. Taken PAP-1 s as example, the total number of perturbations detected is 48,529; perturbations due to the solar activity with Kp $\geq$ 3 stands for 14.5% (7,020/48,529) and ones corresponding to earthquakes for 35.3% (17,112/48,529), which indicates that the number of false alarm stands for 50.2% (24,397/48,529). So the natural ionospheric variations are so important that we have to consider eliminating them in the future work. Additionally, the CSES and DEMETER satellite are at different height orbits. Different heights correspond to different satellite velocity, whose influence on the detection of earthquakes and the duration time of perturbations will also be considered.

Data Availability Statement

The data utilized in this paper are available through the website (http://www.leos.ac.cn/).

Acknowledgments

This work uses data from the CSES mission, a project funded by the China National Space Administration (CNSA) and the China Earthquake Administration (CEA). This work was also supported by the Centre National d'Etudes Spatiales. It is based on observations with the plasma analyzer IAP and the Langmuir probe ISL embarked on DEMETER. This work was supported by the National Key R&D Program of China under Grant No. 2018YFC1503506 and the National Natural Science Foundation of China (NSFC) under Grant No. 41774084.

References

Abdu, M. A., & Batista, I. S. (1977). Sporadic *E*-layer phenomena in the Brazilian magnetic anomaly: Evidence for a regular particle ionization source. *Journal of Atmospheric and Terrestrial Physics*, *39*, 723–732. https://doi.org/10.1016/0021-9169(77)90059-9

Abdu, M. A., Batista, I. S., Carrasco, A. J., & Brum, C. G. M. (2005). South Atlantic magnetic anomaly ionization: A review and a new focus on electrodynamic effects in the equatorial ionosphere. *Journal of Atmospheric and Solar - Terrestrial Physics*, *67*, 1643–1657. https://doi.org/10.1016/j.jastp.2005.01.014

Abdu, M. A., MacDougall, J. W., Batista, I. S., Sobral, J. H. A., & Jayachandran, P. T. (2003). Equatorial evening pre-reversal electric field enhancement and sporadic *E* layer disruption: A manifestation of *E* and *F* region coupling. *Journal of Geophysical Research*, *108*(A6), 1254. https://doi.org/10.1029/2002JA009285

Akhoondzadeh, M., Parrot, M., & Saradjian, M. R. (2010). Electron and ion density variations before strong earthquakes ($M > 6.0$) using DEMETER and GPS data. *Natural Hazards and Earth System Sciences*, *10*(1), 7–18. https://doi.org/10.5194/nhess-10-7-2010

An, Z., Fan, Y., Liu, J., Tan, D., Chen, J., Zheng, G., & Xie, T. (2010). Analysis on ion temperature variation detected by DEMETER before 2008 Wenchuan M_S 8.0 earthquake. *Acta Seismologica Sinica*, *32*(6), 754–759. (in Chinese with English abstract)

Bailey, G. J., Balan, N., & Su, Y. Z. (1997). The Sheffield University plasmasphere-ionosphere model: A review. *Journal of Atmospheric and Terrestrial Physics*, *59*, 1541–1552. https://doi.org/10.1016/S1364-6826(96)00155-1

Balan, N., & Bailey, G. J. (1995). Equatorial plasma fountain and its effects: Possibility of an additional layer. *Journal of Geophysical Research*, *100*(21), 21,421–21,432. https://doi.org/10.1029/95JA01555

Balan, N., Bailey, G. J., Abdu, M. A., Oyama, K. I., Richard, P. G., MacDougall, J., & Batista, I. S. (1997). Equatorial plasma fountain and its effects over three locations: Evidence for an additional layer, the F_3 layer. *Journal of Geophysical Research*, *102*, 2047–2056. https://doi.org/10.1029/95JA02639

Berthelier, J. J., Godefroy, M., Leblanc, F., Seran, E., Peschard, D., Gilbert, P., & Artru, J. (2006). IAP, the thermal plasma analyzer on DEMETER. *Planetary and Space Science*, *54*, 487–501. https://doi.org/10.1016/j.pss.2005.10.018

BŁEÇKI, J., Parrot, M., & Wronowski, R. (2010). Studies of the electromagnetic field variations in ELF frequency range registered by DEMETER over the Sichuan region prior to the 12 May 2008 earthquake. *International Journal of Remote Sensing*, *31*(13), 3615–3629. https://doi.org/10.1080/01431161003727754

Davies, K., & Baker, D. M. (1965). Ionospheric effects observed around the time of the Alaskan earthquake of March 28, 1964. *Journal of Geophysical Research*, *70*, 2251–2253. https://doi.org/10.1029/JZ070i009p02251

Ding, Z. J. W., Sun, S., Chen, J., & Ban, P. (2010). The variation of ionosphere on some days before the Wenchuan Earthquake. *Chinese Journal of Geophysics*, *53*(1), 30–38. https://doi.org/10.3969/j.issn.0001-5733.2010.01.004

Hairston, M. R., Heelis, R., & Rich, F. (1997). Analysis of the ionospheric cross polar cap potential drop and polar ion convection patterns during the January 1997 CME events using DMSP data. *Eos Transactions American Geophysical Union*, *78*, 264.

Hayakawa, M., & Molchanov, O. A. (Eds) (2002). *Seismo–electromagnetics: Lithosphere–atmosphere–ionosphere coupling*. Tokyo: TERRAPUB.

He, Y., Yang, D., Qian, J., & Parrot, M. (2011a). Anomaly of the ionospheric electron density close to earthquakes: Case studies of Pu'er and Wenchuan earthquakes. *Earthquake Science*, *24*(6), 549–555.

He, Y., Yang, D., Qian, J., & Parrot, M. (2011b). Response of the ionospheric electron density to different types of seismic events. *Natural Hazards and Earth System Sciences*, *11*(8), 2173–2180. https://doi.org/10.5194/nhess-11-2173-2011

Horvath, I., & Lovell, B. C. (2009). Distinctive plasma density features of the topside ionosphere and their electrodynamics investigated during southern winter. *Journal of Geophysical Research*, *114*, A01304. https://doi.org/10.1029/2008JA013683

Hsiao, C. C., Liu, J. Y., Oyama, K. I., Yen, N. L., Liou, Y. A., Chen, S. S., & Miau, J. J. (2010). Seismo–ionospheric precursor of the 2008 M_W 7.9 wenchuan earthquake observed by FormoSat–3/COSMIC. *GPS Solutions*, *14*(1), 83–89.

Kendall, P. C., & Pickering, W. M. (1967). Magnetoplasma diffusion at F_2-region altitudes. *Planetary and Space Science*, *15*, 825–833. https://doi.org/10.1016/0032-0633(67)90118-3

Kil, H., DeMajistre, R., Paxton, L. J., & Zhang, Y. (2006). Nighttime F region morphology in the low and middle latitudes seen from DMSP F15 and TIMED/GUVI. *Journal of Atmospheric and Solar - Terrestrial Physics*, *68*, 1672–1681. https://doi.org/10.1016/j.jastp.2006.05.024

Lebreton, J.-P., Stverak, S., Travnicek, P., Maksimovic, M., Klinge, D., Merikallio, S., et al. (2006). The ISL Langmuir probe experiment processing onboard DEMETER: Scientific objectives, description and first results. *Planetary and Space Science*, *54*(5), 472–486. https://doi.org/10.1016/j.pss.2005.10.017

Lefeuvre, F., Rauch, J. L., Lagoutte, D., Berthelier, J. J., & Cerisier, J. C. (1992). Propagation characteristics of dayside low-altitude hiss: Case studies. *Journal of Geophysical Research*, *97*(A7), 10,601–10,620.

Li, M., Lu, J., Zhang, X., & Shen, X. (2019). Indications of ground-based electromagnetic observations to a possible lithosphere–atmosphere–ionosphere electromagnetic coupling before the 12 May 2008 Wenchuan M_S 8.0 earthquake. *Atmosphere*, *10*(7), 355. https://doi.org/10.3390/atmos10070355

Li, M., & Parrot, M. (2012). "Real time analysis" of the ion density measured by the satellite DEMETER in relation with the seismic activity. *Natural Hazards and Earth System Sciences*, *12*(9), 2957–2963. https://doi.org/10.5194/nhess-12-2957-2012

Li, M., & Parrot, M. (2013). Statistical analysis of an ionospheric parameter as a base for earthquake prediction. *Journal of Geophysical Research: Space Physics*, *118*, 3731–3739. https://doi.org/10.1002/jgra.50313

Li, M., & Parrot, M. (2018). Statistical analysis of the ionospheric ion density recorded by DEMETER in the epicenter areas of earthquakes as well as in their magnetically conjugate point areas. *Advances in Space Research*, *61*, 974–984. https://doi.org/10.1016/j.asr.2017.10.047

Li, M., Tan, H., & Cao, M. (2016). Ionospheric influence on the seismo-telluric current related to electromagnetic signals observed before the Wenchuan M_S 8. 0 earthquake. *Solid Earth*, *7*, 1405–1415. https://doi.org/10.5194/se-7-1405-2016

Lin, J., Wu, Y., Zhu, F., Qiao, X., & Zhou, Y. (2009). Wenchuan earthquake ionosphere TEC anomaly detected by GPS. *Chinese Journal of Geophysics*, *52*(1), 297–300. (in Chinese with English abstract).

Liu, C., Guan, Y., Zheng, X., Zhang, A., Piero, D., & Sun, Y. Q. (2018). The technology of space plasma in-situ measurement on the China seismo-electromagnetic satellite. *Science China Technological Sciences*, *62*(5), 829–838. https://doi.org/10.1007/s11431-018-9345-8

Liu, J. Y., Chen, Y. I., Chen, C. H., Liu, C. Y., Chen, C. Y., Nishihashi, M., et al. (2009). Seismoionospheric GPS total electron content anomalies observed before the 12 May 2008 M_W7.9 Wenchuan earthquake. *Journal of Geophysical Research*, *114*, A04320. https://doi.org/10.1029/2008JA013698

Liu, J. Y., Chen, Y. I., Huang, C. C., Parrot, M., Shen, X. H., Pulinets, S. A., et al. (2015). A spatial analysis on seismo–ionospheric anomalies observed by DEMETER during the 2008 *M* 8.0 Wenchuan earthquake. *Journal of Asian Earth Sciences*, *114*, 414–419. https://doi.org/10.1016/j.jseaes.2015.06.012

Liu, J. Y., Chuo, Y. J., Shan, S. J., Tsai, Y. B., Pulinets, S. A., & Yu, S. B. (2009). Preearthquake ionospheric anomalies registered by continuous GPS TEC measurements. *Annales de Geophysique*, *22*(5), 1585–1593.

Ma, X., Lin, Z., Chen, H., Jin, H., Liu, X., & Jiao, L. (2014). Analysis on ionospheric perturbation of TEC and NmF2 based on GPS and COSMIC data before and after the Wenchuan earthquake. *Chinese Journal of Geophysics*, *57*(8), 2415–2422. https://doi.org/10.6038/cjg20140803 in Chinese with English abstract.

Maurya, A. K., Singh, R., Veenadhari, B., Kumar, S., & Singh, A. K. (2013). Sub–ionospheric very low frequency perturbations associated with the 12 May 2008 $M = 7.9$ Wenchuan earthquake. *Natural Hazards and Earth System Sciences*, *13*(9), 2331–2336. https://doi.org/10.5194/nhess-13-2331-2013

Molchanov, O. A., Fedorov, E., Schekotov, A., Gordeev, E., Chebrov, V., Surkov, V., et al. (2004). Lithosphere–atmosphere–ionosphere coupling as governing mechanism for preseismic short–term events in atmosphere and ionosphere. *Natural Hazards and Earth System Sciences*, *4*(5/6), 757–767. https://doi.org/10.5194/nhess-4-757-2004

Molchanov, O. A., & Hayakawa, M. (2008). Seismo electromagnetics and related phenomena: History and latest results, *TERRAPUB*, Tokyo. https://doi.org/10.1016/j.pce.2006.05.001

Němec, F., Santolík, O., & Parrot, M. (2009). Decrease of intensity of ELF/VLF waves observed in the upper ionosphere close to earthquakes: A statistical study. *Journal of Geophysical Research*, *114*, A04303. https://doi.org/10.1029/2008JA013972

Němec, F., Santolík, O., Parrot, M., & Berthelier, J. J. (2008). Spacecraft observations of electromagnetic perturbations connected with seismic activity. *Geophysical Research Letters*, *35*, L05109. https://doi.org/10.1029/2007GL032517

Onishi, T., Berthelier, J. J., & Kamogawa, M. (2011). Critical analysis of the electrostatic turbulence enhancements observed by DEMETER over the Sichuan region during the earthquake preparation. *Natural Hazards and Earth System Sciences*, *11*(2), 561–570. https://doi.org/10.5194/nhess-11-561-2011

Parrot, M. (2011). Statistical analysis of the ion density measured by the satellite DEMETER in relation with the seismic activity. *Earthquake Science*, *24*(6), 513–521. https://doi.org/10.1007/s11589-011-0813-3

Parrot, M. (2012). Statistical analysis of automatically detected ion density variations recorded by DEMETER and their relation to seismic activity. *Annales de Geophysique*, *55*(1), 149–155. https://doi.org/10.4401/ag-5270

Parrot, M., Berthelier, J. J., Lebreton, J. P., Sauvaud, J. A., Santolík, O., & Blecki, J. (2006). Examples of unusual ionospheric observations made by the DEMETER satellite over seismic regions. *Physics and Chemistry of the Earth*, *31*, 486–495. https://doi.org/10.1016/j.pce.2006.02.011

Parrot, M., & Li, M. (2017). Demeter results related to seismic activity. *Ursi Radio Science Bulletin*, *88*(4), 18–25.

Píša, D., Němec, F., Parrot, M., & Santolík, O. (2012). Attenuation of electromagnetic waves at the frequency ~1.7 kHz in the upper ionosphere observed by the DEMETER satellite in the vicinity of earthquakes. *Annales de Geophysique*, *55*(1), 157–163. https://doi.org/10.4401/ag-5276

Píša, D., Němec, F., Santolík, O., Parrot, M., & Rycroft, M. (2013). Additional attenuation of natural VLF electromagnetic waves observed by the DEMETER spacecraft resulting from preseismic activity. *Journal of Geophysical Research: Space Physics*, *118*, 5286–5295. https://doi.org/10.1002/jgra.50469

Pulinets, S. A., Alekseev, V. A., Legen'ka, A. D., & Khegai, V. V. (1997). Radon and metallic aerosols emanation before strong earthquakes and their role in atmosphere and ionosphere modification. *Advances in Space Research*, *20*, 2173–2176. https://doi.org/10.1016/s0273-1177(97)00666-2

Pulinets, S. A., Bondur, V. G., Tsidilina, M. N., & Gaponova, M. V. (2009). Verification of the concept of seismoionospheric coupling under quiet heliogeomagnetic conditions, using the Wenchuan (China) earthquake of May 12, 2008, as an example. *Geomagnetism and Aeronomy*, *50*(2), 231–242.

Pulinets, S. A., Boyarchuk, K. A., Hegai, V., Kim, V. P., & Lomonosov, A. M. (2000). Quasielectrostatic model of atmosphere–thermosphere–ionosphere coupling. *Advances in Space Research*, *26*, 1209–1218. https://doi.org/10.1016/s0273-1177(99)01223-5

Pulinets, S. A., Legen, A. D., Gaivoronskaya, T. V., & Depuev, V. K. (2003). Main phenomenological features of ionospheric precursors of strong earthquakes. *Journal of Atmospheric and Solar - Terrestrial Physics*, *65*, 1337–1347.

Pulinets, S. A., Legen'ka, A. D., & Alekseev, V. A. (1994). *Pre–earthquakes effects and their possible mechanisms, In: Dusty and dirty plasmas, noise and chaos in space and in the laboratory* (pp. 545–557). New York: Plenum Publishing.

Pulinets, S. A., & Ouzounov, D. (2011). Lithosphere–Atmosphere–Ionosphere Coupling (LAIC) model, An unified concept for earthquake precursors validation. *Journal of Asian Earth Sciences*, *41*, 371–382. https://doi.org/10.1016/j.jseaes.2010.03.005

Ryu, K., Parrot, M., Kim, S. G., Jeong, K. S., Chae, J. S., Pulinets, S., & Oyama, K. I. (2014). Suspected seismo–ionospheric coupling observed by satellite measurements and GPS TEC related to the *M*7.9 Wenchuan earthquake of 12 May 2008. *Journal of Geophysical Research: Space Physics*, *119*, 305–323. https://doi.org/10.1002/2014JA020613

Sarkar, S., & Gwal, A. K. (2010). Satellite monitoring of anomalous effects in the ionosphere related to the great Wenchuan earthquake of May 12, 2008. *Natural Hazards and Earth System Sciences*, *55*(2), 321–332. https://doi.org/10.1007/s11069-010-9530-9

Savitzky, A., & Golay, M. J. E. (1964). Smoothing and differentiation of data by simplified least squares procedures. *Analytical Chemistry*, *36*, 1627–1639.

Shen, X., Zhang, X., Yuan, S., Wang, L., Cao, J., Huang, J., et al. (2018). The state-of-the-art of the China Seismo-Electromagnetic Satellite mission. *Science China Technological Sciences*, *61*(5), 634–642. https://doi.org/10.1007/s11431-018-9242-0

Silina, A. S., Liperovskaya, E. V., Liperovsky, V. A., & Meister, C.-V. (2001). Ionospheric phenomena before strong earthquakes. *Natural Hazards and Earth System Sciences*, *1*(3), 113–118. https://doi.org/10.5194/nhess-1-113-2001

Sorokin, V., Chemyrev, V., & Hayakawa, M. (2015). Electrodynamic coupling of lithosphere–atmosphere–ionosphere of the Earth, Nova Science Pub. Inc. https://doi.org/10.1016/j.jseaes.2010.03.005

Stangl, G., & Boudjada, M. Y. (2011). Investigation of TEC and VLF space measurements associated to L'Aquila (Italy) earthquakes. *Natural Hazards and Earth System Sciences*, *11*(4), 1019–1024. https://doi.org/10.5194/nhess-11-1019-2011

Sun, Y., Oyama, K. I., Liu, J. Y., Jhuang, H. K., & Cheng, C. Z. (2011). The neutral temperature in the ionospheric dynamo region and the ionospheric *F* region density during Wenchuan and Pingtung Doublet earthquakes. *Natural Hazards and Earth System Sciences*, *11*(6), 1759–1768. https://doi.org/10.5194/nhess-11-1759-2011

Titheridge, J. E. (1995). Winds in the ionosphere—A review. *Journal of Atmospheric and Terrestrial Physics*, *57*, 1681–1714. https://doi.org/10.1016/0021-9169(95)00091-F

Trivedi, N. B., Pathan, B. M., Schuch, N. J., Barreto, M., & Dutra, L. G. (2005). Geomagnetic phenomena in the South Atlantic anomaly region in Brazil. *Advances in Space Research*, *36*, 21–24. https://doi.org/10.1016/j.asr.2004.09.020

Walker, S. N., Kadirkamanathan, V., & Pokhotelov, O. A. (2013). Changes in the ultra–low frequency wave field during the precursor phase to the Sichuan earthquake: DEMETER observations. *Annales de Geophysique*, *31*, 1597–1603. https://doi.org/10.5194/angeo-31-1597-2013

Wan, J., Wang, F., Shan, X., & Yan, X. (2012). Preliminary application of energetic particle on DEMETER Satellite in Wenchuan earthquake. *Progress in Geophysics*, *27*(6), 2279–2288. (in Chinese with English abstract).

Xu, T., Hu, Y., Wu, J., Wu, Z., Suo, Y., & Feng, J. (2010). Giant disturbance in the ionospheric F_2 region prior to the *M* 8.0 Wenchuan earthquake on 12 May 2008. *Annales Geophysicae*, *28*, 1533–1538. https://doi.org/10.5194/angeo-28-1533-2010

Xu, T., Hu, Y., Wu, Z., Suo, Y., Feng, J., & Huang, C. (2010). Abnormal perturbations in the ionospheric F_2 region before Wenchuan earthquake on 12 May 2008. *Science in China Series D: Earth Sciences*, *53*(11), 1671–1674. https://doi.org/10.1007/s11430-010-4046-4

Xu, T., Wu, J., Zhao, Z., Liu, Y., He, S., Li, J., et al. (2011). Brief communication "Monitoring ionospheric variations before earthquakes using the vertical and oblique sounding network over China". *Natural Hazards and Earth System Sciences*, *11*(4), 1083–1089. https://doi.org/10.5194/nhess-11-1083-2011

Yan, R., Guan, Y., Shen, X., Huang, J., Zhang, X., Liu, C., & Liu, D. (2018). The Langmuir Probe onboard CSES: Data inversion analysis method and first results. *Earth and Planetary Physics*, *2*, 479–488. https://doi.org/10.26464/epp2018046

Yan, R., Parrot, M., & Pinçon, J. L. (2017). Statistical study on variations of the ionospheric ion density observed by DEMETER and related to seismic activities. *Journal of Geophysical Research: Space Physics*, *122*, 12,421–12,429. https://doi.org/10.1002/2017JA024623

Yan, X., Shan, X., Cao, J., Tang, J., & Wang, F. (2012). Seismoionospheric anomalies observed before the Wenchuan earthquake using GPS and DEMETER data. *Seismology and Geology*, *34*(1), 160–171. https://doi.org/10.3969/j.issn.0253-4967.2012.01.015

Yu, T., Mao, T., Wang, Y. G., & Wang, J. S. (2009). Study of the ionospheric anomaly before the Wenchuan earthquake. *Chinese Science Bulletin*, *54*(6), 1086–1092. CNKI:SUN:JXTW.0.2009-06-026 (in Chinese with English abstract).

Zeng, Z., Zhang, B., Fang, G., Wang, D., & Yin, H. (2009). The analysis of ionospheric variations before Wenchuan earthquake with DEMETER data. *Chinese Journal of Geophysics*, *52*(1), 11–19. (in Chinese with English abstract).

Zhang, X., Fidani, C., Huang, J., Shen, X., Zeren, Z., & Qian, J. (2013). Burst increases of precipitating electrons recorded by the DEMETER satellite before strong earthquakes. *Natural Hazards and Earth System Sciences*, *13*(1), 197–209. https://doi.org/10.5194/nhess-13-197-2013

Zhang, X., Shen, X., Liu, J., Ouyang, X., Qian, J., & Zhao, S. (2009). Analysis of ionospheric plasma perturbations before Wenchuan earthquake. *Natural Hazards and Earth System Sciences*, *9*(4), 1259–1266. https://doi.org/10.5194/nhess-9-1259-2009

Zhang, X., Shen, X., Ouyang, X., Cai, J., Huang, J., Liu, J., & Zhao, S. (2009). Ionosphere VLF electric field anomalies before Wenchuan *M* 8 earthquake. *Chinese Journal of Radio Science*, *24*(6), 1024–1032. (in Chinese with English abstract).

Zhao, B., Wang, M., Yu, T., Xu, G., Wan, W., & Liu, L. (2010). Ionospheric total electron content variations prior to the 2008 Wenchuan Earthquake. *International Journal of Remote Sensing*, *31*(13), 3545–3557. https://doi.org/10.1080/01431161003727622

Zhao, B., Yu, T., Wang, M., Wan, W., Lei, J., Liu, L., & Ning, B. (2008). Is an unusual large enhancement of ionospheric electron density linked with the 2008 great Wenchuan earthquake? *Journal of Geophysical Research*, *113*, A11304. https://doi.org/10.1029/2008JA013613

Zhu, F., Wu, Y., Lin, J., Zhou, Y., Xiong, J., & Yang, J. (2009). Anomalous response of ionospheric VTEC before the Wenchuan earthquake. *Acta Seismologica Sinica*, *31*(2), 180–187.